

Performance Monitoring for Live Systems with Soft FEC and Multilevel Modulation

Tsuyoshi Yoshida, *Member, IEEE*, Mikael Mazur, *Member, IEEE*, Jochen Schröder, *Member, IEEE*, Magnus Karlsson, *Fellow, OSA; Senior Member, IEEE*, and Erik Agrell, *Fellow, IEEE*

(Top-Scored)

Abstract—Performance monitoring is an essential function for margin measurements in live systems. Historically, system budgets have been described by the Q-factor converted from the bit error rate (BER) under binary modulation and direct detection. The introduction of hard forward error correction (FEC) did not change this. In recent years, technologies have changed significantly to comprise coherent detection, multilevel modulation and soft FEC. In such advanced systems, different metrics such as (normalized) generalized mutual information (GMI/NGMI) and asymmetric information (ASI) are regarded as being more reliable. On the other hand, Q budgets are still useful because pre-FEC BER monitoring is established in industry for live system monitoring.

The pre-FEC BER is easily estimated from available information of the number of flipped bits in the FEC decoding, which does not require knowledge of the transmitted bits that are unknown in live systems. Therefore, the use of metrics like GMI/NGMI/ASI for performance monitoring has not been possible in live systems. However, in this work we propose a blind soft-performance estimation method. Based on a histogram of log-likelihood-values without the knowledge of the transmitted bits, we show how the ASI can be estimated.

We examine the proposed method experimentally for 16- and 64-ary quadrature amplitude modulation (QAM) and probabilistically shaped 16-, 64-, and 256-QAM in recirculating loop experiments. We see a relative error of 3.6%, which corresponds to around 0.5 dB signal-to-noise ratio difference for binary modulation, in the regime where the ASI is larger than the assumed FEC threshold. For this proposed method, the digital signal processing circuitry requires only the minimal additional function of storing the L-value histograms before the soft FEC decoder.

Index Terms—Bit error rate, bitwise decoding, forward error correction, modulation, mutual information, optical fiber communication, performance monitoring, probabilistic shaping.

Manuscript received November 15, 2019; revised February 4, 2020. This work was partly presented at ECOC 2019 [29].

This work was funded in part by “Massive Parallel and Sliced Optical Network (MAPLE),” the Commissioned Research of National Institute of Information and Communications Technology (NICT), Japan (project number 20401), and the Swedish Research Council, VR (grant 2014-06138).

T. Yoshida is with Information Technology R&D Center, Mitsubishi Electric Corporation, Kamakura, 247-8501 Japan (e-mails: Yoshida.Tsuyoshi@ah.MitsubishiElectric.co.jp). He also belongs to Osaka University, Suita, Osaka, 505-0871 Japan.

M. Mazur, J. Schröder, M. Karlsson, and E. Agrell are with the Fiber-Optic Communications Research Center (FORCE), Chalmers University of Technology, SE-41296 Gothenburg, Sweden.

Copyright (c) 2020 IEEE. Personal use of this material is permitted. However, permission to use this material for any other purposes must be obtained from the IEEE by sending a request to pubs-permissions@ieee.org.

I. INTRODUCTION

Optical fiber communications are expected to carry traffic at high data rates with high reliability. Thus a very low bit error rate (BER) is required, such as 10^{-9} or 10^{-12} in early systems and currently 10^{-15} [1]. Following a standard [2], system vendors have used margins from the threshold Q-factor converted from the corresponding BER to cope with potential extra impairments due to fiber nonlinearity, polarization/wavelength-dependent phenomena, system aging and variation, component imperfections, etc. In recent years, there has been a trend to reduce margin allocation for efficient networking in cases of dynamic network reconfiguration [3]. Then, real-time performance monitoring, whose trends are well summarized in [4], is becoming more important than ever. When examining the performance with known test bits, one can easily quantify the performance at the receiver. However, once the system starts to carry live traffic, the true transmitted bits are unknown at the receiver. Then, the performance must be monitored blindly, without knowledge of the transmitted data. Optical spectrum analysis is one of the key instruments that can establish the system status. More recently, optical modulation analyzers have become essential in optical transceiver production. However, to install such instruments for entire systems is unrealistic due to cost reasons. Thus there have been many studies of performance monitoring with minimal or low-cost hardware since the days of on-off keying modulated (OOK) systems. The main monitoring target can be for example optical signal-to-noise ratio (OSNR) or chromatic and polarization-mode dispersion [5]. Neural networks have been proposed for such monitoring and also applied to detect imperfect modulation in the transmitter [6]. Monitoring with coherent detection was proposed for direct-detection systems [7], and after the deployment of coherent communications with digital signal processing (DSP), the digital coherent receiver is used for performance monitoring [8]. In-band OSNR monitoring [9], [10] is also important, partly because it is inaccessible to conventional optical spectrum analyzers. Further, in dense wavelength division multiplexing with channel spacing close to Nyquist limit, the optical background noise can be difficult to estimate [11]. Another important topic is to distinguish the noise from amplified spontaneous emission (ASE) and nonlinear noise, such as broadband four-wave mixing under nonlinear fiber-optic transmission [12], which has been studied extensively [13], [14]. Very recently, data-analysis-based power profile estimation over multiple spans was demonstrated

[15].

Among the various targets of performance monitoring, the BER is one of the most basic and essential ones in network operation. For systems with OOK without forward error correction (FEC) with a few dBs of system margin, the BER is usually too low to be measurable in a reasonable time. Thus the BER or the corresponding Q-factor at the optimum decision threshold was estimated from the BERs using nonideal decision thresholds, also called “bath-tub curves” [16]. Alternatively, the Q-factor could be estimated from the statistics (mean and standard deviations) of the eye-diagram. Since the deployment of systems with hard FEC [17], the performance has been quantified by the pre-FEC BER (or Q-factor) and compared with the boundary value required for quasi-error-free transmission after FEC decoding, the so-called *FEC limit*. A pre-FEC BER is then estimated by the bit flipping ratio in the FEC decoder.

In the last decade, coherent detection, DSP [18], soft FEC [19] and multilevel modulation have been widely deployed, as summarized in [20]. More recently, probabilistic shaping (PS) with reverse concatenation [21], [22] have gained much attention for its capacity-approaching performance. Then more reliable performance metrics to predict post-FEC performance must be considered. At the same time, information-theoretic metrics such as mutual information (MI) [23], generalized MI (GMI) [24], normalized GMI (NGMI) [25], achievable binary code (ABC) rate [26], and asymmetric information (ASI) [27], achievable FEC rate [28] have been introduced. To compute these metrics, the transmitted bits must be known, and their application to performance monitoring in live systems without this knowledge is not straightforward. At typical operation points, which are near or beyond the “waterfall region” of modern soft FEC codes, the SNR can be relatively low, e.g., 10 dB, which can make the performance estimate unreliable. It is thus valuable to verify and quantify in simulations and experiments the accuracy of these modern performance metrics in a context with powerful codes operating at relatively low SNR levels.

This work is an invited extension of [29]. We propose a performance-monitoring technique applicable to systems carrying live traffic with soft FEC and multilevel modulation such as high-order quadrature amplitude modulation (QAM) under bitwise decoding. We estimate the ASI, which is known as a good predictor of post-FEC BER with soft FEC, multilevel modulation, and PS [27], [30]. The proposed estimation method is validated experimentally using various combinations of modulation formats and shaping codes. The main extensions from [29] lie in a more detailed theoretical background, additional examinations under different FEC thresholds and launch powers, Q-factor estimation based on slightly modified and improved statistics, and additional back-to-back experimental results to investigate the cause of the estimation errors.

This paper is organized as follows: Sec. II describes the theoretical background required to understand the proposed method, which is then presented in Sec. III. Sec. IV describes the experiment and the results, and Sec. V concludes the work.

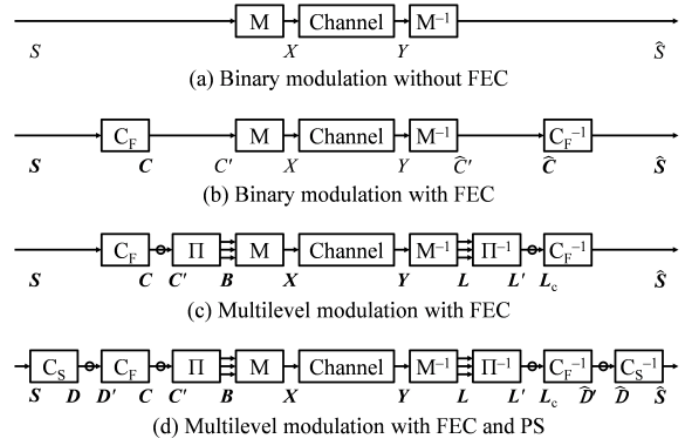


Fig. 1. System models: (a) binary modulation without FEC, (b) binary modulation with FEC, (c) multilevel modulation with FEC, and (d) multilevel modulation with FEC and PS. The functions M , C_F , Π , and C_S are symbol mapping, FEC encoding, bit-interleaving, and PS encoding at the transmitter. The functions at the receiver are their inverse operations.

II. PRELIMINARIES

In this section, we summarize system models and relevant performance metrics for, first, legacy systems with OOK, direct detection and hard FEC, and second, more modern systems with coherent detection and possibly high-order QAM, PS and soft FEC. Fig. 1 shows some typical deployable system models. The models and performance metrics for binary modulation are explained in Sec. II-A, and those for multilevel modulation in Sec. II-B, respectively.

A. Performance in systems with binary modulation

Optical fiber communications have supported binary modulation for a long time, such as OOK, differential binary/quaternary phase-shift keying (BPSK/QPSK), and coherent BPSK/QPSK with polarization-division multiplexing. Fig. 1(a) shows the system model for binary modulation without FEC, which was employed for OOK systems. The source bits $S \in \mathbb{B}$ are mapped into binary symbols $X \in \mathbb{R}$, and received symbols $Y \in \mathbb{R}$ are demapped into estimated bits $\hat{S} \in \mathbb{B}$, where \mathbb{B} and \mathbb{R} denote the binary number set and the real number set, respectively. Such early systems were not equipped with FEC, but the raw BER had to be quasi-error-free, which in practice meant lower than 10^{-9} or 10^{-12} , while 10^{-15} is the target in the most recent standards. To quantify such a low BER easier or more intuitively, the BER was converted into the (SNR-like) Q-factor

$$Q_{\text{BER}} \triangleq \sqrt{2} \operatorname{erfc}^{-1}(2 \cdot \text{BER}). \quad (1)$$

The Q-factor Q_{BER} shows more linear relationship with (the electrical) signal-to-noise ratio (SNR) and OSNR than the BER. For uniform binary modulation, Q_{BER}^2 gives the SNR required for a given BER over the Gaussian channel. Historically, the Q-factor was related to the eye-opening of binary modulation. From the mean μ_b (denoting the average location of the upper and lower “rails” of the eye diagram) and standard deviation σ_b (representing the width of said rails)

of the sampled signals for the transmitted bits $b \in \mathbb{B}$, the “statistical” Q-factor was defined as

$$Q_{\text{st}} \triangleq \frac{|\mu_0 - \mu_1|}{\sigma_0 + \sigma_1}. \quad (2)$$

In the case of uniform binary modulation over the Gaussian channel, $Q_{\text{st}} = Q_{\text{BER}}$. While this holds for a thermal-noise-limited channel, a direct-detection optical channel limited by ASE noise is non-Gaussian, with a noncentral chi-square distribution, making $Q_{\text{st}} \neq Q_{\text{BER}}$.¹ There are many performance monitoring methods for OOK from such statistics. Without the knowledge of the transmitted bits, μ_b and σ_b are estimated as $\hat{\mu}_b$ and $\hat{\sigma}_b$, based on an assumed suitable decision criterion to estimate the transmitted bit b for each sample. Then the statistical Q-factor can be estimated as

$$\hat{Q}_{\text{st}} \triangleq \frac{|\hat{\mu}_0 - \hat{\mu}_1|}{\hat{\sigma}_0 + \hat{\sigma}_1} \approx Q_{\text{st}}, \quad (3)$$

which could be obtained directly from the eye diagram measured by an oscilloscope, and hence became a popular system quality metric due to its simplicity. When the BER is less than 10^{-9} , the estimated statistics $\hat{\mu}_b$ and $\hat{\sigma}_b$, and the resulting estimated Q-factor \hat{Q}_{st} are reliable.

With increased throughput, FEC was introduced for efficiency and reliability [17], [19]. Fig. 1(b) shows the system model in that case. At the transmitter, source bits $\mathbf{S} \in \mathbb{B}^k$ are encoded by the FEC into $\mathbf{C} \in \mathbb{B}^n$, where n and k now denote the FEC codeword length and the number of information bits, respectively. The encoded bits $\mathbf{C}' \in \mathbb{B}$ are then mapped into binary symbols $\mathbf{X} \in \mathbb{R}$. At the receiver, the received symbols $\mathbf{Y} \in \mathbb{R}$ are demapped into the estimated encoded bits $\hat{\mathbf{C}}' \in \mathbb{B}$.² The estimated encoded bits for a FEC codeword $\hat{\mathbf{C}} \in \mathbb{B}^n$ are decoded into the estimated source bits $\hat{\mathbf{S}} \in \mathbb{B}^k$. In this system, the relevant performance metric is now the BER after FEC decoding³, or post-FEC BER,

$$BER_{\text{post}} \triangleq \sum_{b \in \mathbb{B}} P_{S, \hat{S}}(b, 1 - b), \quad (4)$$

where (S, \hat{S}) denotes a random pair of bits in $(\mathbf{S}, \hat{\mathbf{S}})$ and $P_{S, \hat{S}}(b, 1 - b)$ denotes the joint probability of $S = b$ and $\hat{S} = 1 - b$. Recent system requirements on BER_{post} can be as low as 10^{-15} . However, to measure such a low BER_{post} in real time is difficult and time-consuming. Instead, the BER before FEC decoding, the pre-FEC BER,

$$BER_{\text{pre}} \triangleq \sum_{b \in \mathbb{B}} P_{C, \hat{C}}(b, 1 - b), \quad (5)$$

where (C, \hat{C}) denotes a random pair of bits in $(\mathbf{C}, \hat{\mathbf{C}})$, is often measured and converted into a Q-factor by (1). Since BER_{pre} is usually higher in systems with FEC than in systems without FEC, estimating the Q-factor via (3) is less reliable.

¹In coherent BPSK/QPSK systems, the Gaussian channel model is applicable even with optical amplifiers.

²In most cases, hard FEC has been employed in systems with binary modulation, including 100 Gb/s coherent detection systems, while long-reach coherent BPSK/QPSK systems employed soft FEC [19]. Then, the received symbols \mathbf{Y} are demapped into L-values as shown in Sec. II-B.

³If PS is employed, the BER after PS decoding, if that is placed after the FEC decoding, is more relevant [31]–[33].

A threshold value of BER_{pre} into the FEC decoder for error-free operation is also characterized in the FEC design and called the *Q limit*. In the standardized Q budget [2], the starting point is Q_{BER} at a given received OSNR at the beginning-of-life of the system, and the penalties are then quantified relative to this Q-factor, never to reach the Q limit before the system’s end-of-life.

B. Performance in systems with soft binary FEC and multi-level modulation

Fig. 1(c) shows the system model for multilevel modulation with soft binary FEC, i.e., bit-interleaved coded modulation (BICM) [34]–[37]. This system model is relevant for 400 Gb/s standards of 400ZR [38] and openROADM [39], e.g., 400 Gb/s 16-QAM with concatenated (soft) Hamming and (hard) staircase codes [40]. This BICM system can be further generalized to include PS in Fig. 1(d), so in the following we describe Fig. 1(d). Source bits $\mathbf{S} \in \mathbb{B}^{k_{\text{ps}}}$ are encoded into $\mathbf{D} \in \mathbb{B}^{n_{\text{ps}}}$ by PS encoding. After reframing, the PS-encoded bits $\mathbf{D}' \in \mathbb{B}^k$ are encoded by FEC into the bits $\mathbf{C} \in \mathbb{B}^n$. The FEC-encoded bits $\mathbf{C}' \in \mathbb{B}^m$ are interleaved into bits $\mathbf{B} = (B_1, \dots, B_m) \in \mathbb{B}^m$, where m denotes the number of bits per complex symbol. The bits \mathbf{B} are mapped into symbols $\mathbf{X} \in \mathbb{R}^2$.

In the receiver, the received symbols \mathbf{Y} are demapped into L-values $\mathbf{L} = (L_1, \dots, L_m) \in \mathbb{L}^m$ as [37, Eqs. (3.31)–(3.32), (3.39)]

$$L_i(\mathbf{y}) \triangleq \left\lfloor \ln \frac{q_{B_i, \mathbf{Y}}(0, \mathbf{y})}{q_{B_i, \mathbf{Y}}(1, \mathbf{y})} \right\rfloor_{\mathbb{L}}, \quad (6)$$

where $\lfloor l \rfloor_{\mathbb{L}}$ denotes quantization of a real number l to the nearest value in \mathbb{L} , and $q_{B_i, \mathbf{Y}}(b, \mathbf{y})$ is the joint probability distribution assumed in the demapper. It can be factorized as $q_{B_i, \mathbf{Y}}(b, \mathbf{y}) = P_{B_i}(b)q_{\mathbf{Y}|B_i}(\mathbf{y} | b)$, where $P_{B_i}(b)$ denotes the probability of bit B_i being b and $q_{\mathbf{Y}|B_i}(\mathbf{y} | b)$ is the auxiliary channel assumed in the demapper. Furthermore, the demapping function quantizes both the input symbols \mathbf{Y} (to typically 64 to 1024 levels in each dimension) and output L-values \mathbf{L} , using uniform mid-rise quantization. Specifically, the discrete set of L-values is $\mathbb{L} \triangleq \{-l_{\text{max}}, -l_{\text{max}} + \Delta l, -l_{\text{max}} + 2\Delta l, \dots, l_{\text{max}}\}$, where $l_{\text{max}} \triangleq (n_{\text{bin}} - 1)\Delta l/2$, n_{bin} is the number of bins, and Δl is the step size.

After deinterleaving \mathbf{L} into $\mathbf{L}' \in \mathbb{L}^m$ and framing, the L-values per FEC codeword $\mathbf{L}_c \in \mathbb{L}^n$ are decoded by the FEC decoder into $\mathbf{D} \in \mathbb{B}^k$. The decoded bits per PS codeword $\hat{\mathbf{D}}' \in \mathbb{B}^{n_{\text{ps}}}$ are decoded by the PS decoder into the estimated source bits $\hat{\mathbf{S}} \in \mathbb{B}^{k_{\text{ps}}}$. If there is no PS coding, $k_{\text{ps}} = k$, then the source bits \mathbf{S} are fed directly into the FEC encoder, and the FEC decoder output gives the estimated source bits $\hat{\mathbf{S}}$.

In analogy with (4), the post-FEC BER for systems with BICM and PS is $BER_{\text{post}} = \sum_{b \in \mathbb{B}} P_{D', \hat{D}'}(b, 1 - b)$, where (D', \hat{D}') denotes a random pair of bits in $(\mathbf{D}', \hat{\mathbf{D}}')$. As predictors of the post-FEC BER under BICM with PS, more useful metrics than pre-FEC BER (or Q_{BER}) are NGMI [25], [41], ABC rate [26], ASI [27], and achievable FEC rate [28]. The post-FEC BER curves were compared in [25], [27], [42], [43]. They are all equivalent under matched decoding but

not under mismatched decoding [42]. The difference between NGMI and ASI was first observed in [30]. The definitions of GMI [44, Eq. (20)], [24, Eq. (21)], NGMI [25, Eq. (6)], [41, Eq. (14)], and ASI I_a [27, Eq. (11)] are

$$GMI \triangleq \max_{s>0} I_{q,s}^{\text{gmi}}(\mathbf{B}; \mathbf{Y}), \quad (7)$$

$$I_{q,s}^{\text{gmi}}(\mathbf{B}; \mathbf{Y}) \triangleq \mathbb{E}_{\mathbf{B}, \mathbf{Y}} \left[\log_2 \frac{q_{\mathbf{Y}|\mathbf{B}}(\mathbf{y}|\mathbf{b})^s}{\sum_{\mathbf{b} \in \mathbb{B}^m} P_{\mathbf{B}}(\mathbf{b}) q_{\mathbf{Y}|\mathbf{B}}(\mathbf{y}|\mathbf{b})^s} \right], \quad (8)$$

$$NGMI \triangleq 1 - \frac{1}{m} (\mathbb{H}(\mathbf{B}) - GMI), \quad (9)$$

$$I_a \triangleq 1 - \mathbb{H}(L_a | |L_a|), \quad (10)$$

where $\mathbb{H}(\cdot)$ and $\mathbb{E}[\cdot]$ denote entropy and expectation. L_a is the symmetrized *a posteriori* L-values $L_a \triangleq (-1)^b L$, where $L = L_I$ for a random bit tributary I , selected uniformly from $\{1, \dots, m\}$, and b is the corresponding transmitted bit in B_I [24, Eq. (33)], [27, Eq. (10)].⁴ In a bitwise receiver, which we assume in this paper, the channel assumed in the demapper $q_{\mathbf{Y}|\mathbf{B}}(\mathbf{y}|\mathbf{b})$ is [22, Eq. (22)]

$$q_{\mathbf{Y}|\mathbf{B}}(\mathbf{y}|\mathbf{b}) = \frac{1}{P_{\mathbf{B}}(\mathbf{b})} \prod_{i=1}^m q_{B_i, \mathbf{Y}}(b_i, \mathbf{y}), \quad (11)$$

where $\mathbf{b} = (b_1 b_2 \dots b_m)$. The scaling parameter s controls the auxiliary channel, and the optimum s (s_o) gives the GMI as $I_{q,s_o}(\mathbf{B}; \mathbf{Y})$. The NGMI and the ASI are equivalent under matched decoding ($s_o = 1$), but not necessarily so under mismatched decoding ($s_o \neq 1$) [27]. Furthermore, it can be shown that the NGMI is equivalent to the ABC rate under matched decoding [42]. As an example of a practical implementation, the SNR of the auxiliary channel is set to a fixed FEC threshold value, as in [45]. Then there may be a gap of up to several dBs between the SNRs of the received symbols carrying live traffic and that of the auxiliary channel [42]. The ASI is computed from such mismatched and quantized L-values, and it characterizes the performance just before the FEC decoder in deployable systems.

III. PROPOSED METHOD

In this section we explain the configuration of the receiver side DSP and the operation principle of the proposed blind ASI monitoring method.

A. Configuration

Fig. 2 shows the functions around the bitwise FEC decoding in the DSP, which is a part of Fig. 1(c) or 1(d). This figure explains both the usual derivation of information-theoretic performance metrics and the proposed performance monitoring paths. Usually GMI, NGMI, and ASI are computed with the knowledge of the transmitted bits \mathbf{B} . In our proposed technique, we aim to estimate the ASI without this knowledge. We add a memory for storing a histogram of L-values before the FEC decoding, and then extract the histogram to an external function using offline software or a field programmable gate

⁴In [24], [27], the L-values were defined over the set of real numbers, whereas in this paper, we define them over the discrete set \mathbb{L} . Therefore, entropy is used in (10) instead of differential entropy as in [27].

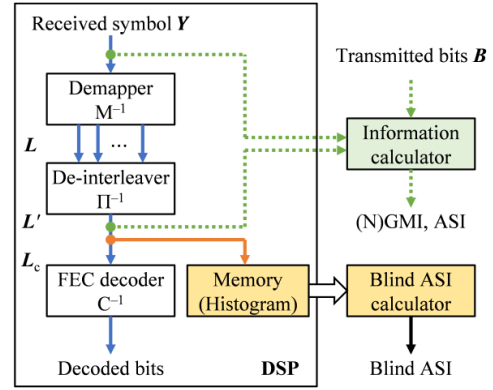


Fig. 2. Typical computation of information-theoretic performance metrics (green) and functions for performance monitoring of live systems (orange and yellow) around the FEC decoding in DSP.

array, and derive a *blind* estimate of the ASI. Although we could have used the received symbol \mathbf{Y} instead of L' , any approximation or mismatch in the demapping would then not have been accounted for.

B. Principle

Fig. 3 shows an example of an L-value histogram for PS-64-QAM at an SNR of 10 dB. Constant-composition distribution matching [46] was used to shape the incoming bits into symbols \mathbf{X} , having a symbol entropy $\mathbb{H}(\mathbf{B}) = 4.1$ bits per channel use (bpcu) and a PS codeword length $n_{\text{ps}} = 1024$ one-dimensional 8-ary pulse amplitude modulation symbols. We employed more than 10^6 samples of the L-values to quantify the performance.

The ASI can be computed according to (10) if the probability mass function (pmf) P_{L_a} (yellow curve in Fig. 3(a)) is known. However, under the condition that the transmitted bit b is unknown, the symmetrized L-values L_a are also unknown. However, the pmf $P_{|L_a|}(l) = P_{|L|}(l)$ (orange curve in Figs. 3(a) and 3(b)) is known even if b is unknown. Based on real-time measurements of $|L| = |L_a|$, which is quantized to the nearest bin in \mathbb{L} as in (6), we construct a histogram $P_{|L_a|}(l)$, $l \in \mathbb{L}$. Due to the finite range of \mathbb{L} , there is a peak at $P_{|L_a|}(l_{\text{max}})$, which represents quantizer overload in (6).

We assume at least the left-side tail of P_{L_a} , which mainly determines the ASI, follows a Gaussian distribution. We therefore precompute a set of discretized Gaussian distributions $P_{G_k}^t$ ($k = 1, \dots, K$) and their corresponding symmetrized pmfs $P_{|G_k|}^t$. By comparing $P_{|G_k|}^t$ (green curve in Fig. 3) with the histogram $P_{|L_a|}$ (orange), the best distribution $P_{G_k}^t$ is chosen as the estimated pmf \hat{P}_{L_a} . The procedure can be summarized as follows:

- 1) Select a set of Gaussian distributions⁵ $f_k(l) \triangleq \exp[-(l - \mu[k])^2 / (2\sigma^2[k])]$ for $k = 1, \dots, K$ and discretize them into

$$P_{G_k}^t(l) \triangleq \begin{cases} \int_{l-\Delta l/2}^{l+\Delta l/2} f_k(l) dl, & l \in \mathbb{L} \setminus \{-l_{\text{max}}, l_{\text{max}}\}, \\ \int_{-\infty}^{-l_{\text{max}}+\Delta l/2} f_k(l) dl, & l = -l_{\text{max}}. \end{cases} \quad (12)$$

⁵The constant factor and $P_{G_k}(l_{\text{max}})$ can be chosen arbitrarily, since these will not be used in (13)–(17).

- 2) Set $\rho \triangleq P_{|L_a|}(l_{\max})$.
- 3) For $k = 1, 2, \dots, K$, let

$$P_{G_k^*}(l) \triangleq \begin{cases} \frac{1-\rho}{\sum_{l' \in \mathbb{L} \setminus \{l_{\max}\}} P_{G_k}(l')} P_{G_k}(l), & l \in \mathbb{L} \setminus \{l_{\max}\}, \\ \rho, & l = l_{\max}, \end{cases} \quad (13)$$

where the normalization serves to satisfy $\sum_{l \in \mathbb{L}} P_{G_k^*}(l) = 1$, and calculate $P_{|G_k^*|}(l) = P_{G_k^*}(-l) + P_{G_k^*}(l)$ for $l \in \mathbb{L}^+ = \{l \in \mathbb{L} : l > 0\}$.

- 4) Find by full search

$$\hat{k} \triangleq \arg \min_k \sum_{l \in \mathbb{L}^+} \left(P_{|L_a|}(l) - P_{|G_k^*|}(l) \right)^2. \quad (14)$$

Other optimization methods, e.g., gradient descent over the distribution parameters, can be employed instead.

- 5) Assume that the parameters $\mu[\hat{k}]$ and $\sigma[\hat{k}]$ estimated for $|L| = |L_a|$ also are valid for L_a ; i.e., set

$$\hat{P}_{L_a}(l) \triangleq P_{G_{\hat{k}}^*}(l), \quad l \in \mathbb{L}. \quad (15)$$

- 6) Calculate an estimate of the ASI, called *blind* ASI and denoted \hat{I}_a in the remains of this paper, by (10), using \hat{P}_{L_a} to approximate P_{L_a} .

- 7) Optionally, an estimate of the Q-factor

$$\hat{Q}_{\text{st},L} = \text{erfc}^{-1} \left(2(1-\rho) \widehat{BER}_{\text{Gauss}} \right) \quad (16)$$

can be computed as a by-product, where,

$$\widehat{BER}_{\text{Gauss}} = \frac{1}{2} \text{erfc} \left(\frac{\mu[\hat{k}]}{\sqrt{2}\sigma[\hat{k}]} \right). \quad (17)$$

In (17), the factor $(1-\rho)$ removes the influence of the peak due to quantization overload in the histogram of L-values, which we did not consider in [29].

C. Initial simulation

In Fig. 3, the ASI from the sampled $P_{|L_a|}$ using knowledge of the transmitted bits, I_a , is 0.876 and that from the proposed estimation method, \hat{I}_a , is 0.870, so the absolute estimation error is 0.006. Fig. 4 shows the absolute estimation errors of the ASI by the proposed method with different resolutions of the L-value histogram from $n_{\text{bin}} = 16$ to 256 bins (4 to 8 bits). The resolution is the same as for the L-values fed into the soft FEC decoder. The I_a was changed along the horizontal axis by sweeping the SNR from 5 dB to 15 dB. The SNR of the auxiliary channel was set to an FEC threshold condition of $I_a = 0.86$ [47], which corresponds to a Q_{BER} of 5 dB for QPSK over the Gaussian channel. Note that there are random fluctuations between simulation instances, and that a coarse quantization with a small number of bins degrades the signal quality of I_a . With at least 32 bins, the reduction is negligible. In Fig. 3, in the regime where I_a is more than the FEC threshold (here 0.86) is much more important than the others for the system margin estimation. In this regime, the estimation errors for the examined bin sizes (with fluctuations between simulation instances) are not significantly different. The absolute estimation errors are within 0.015, giving a relative error of 1.7%.

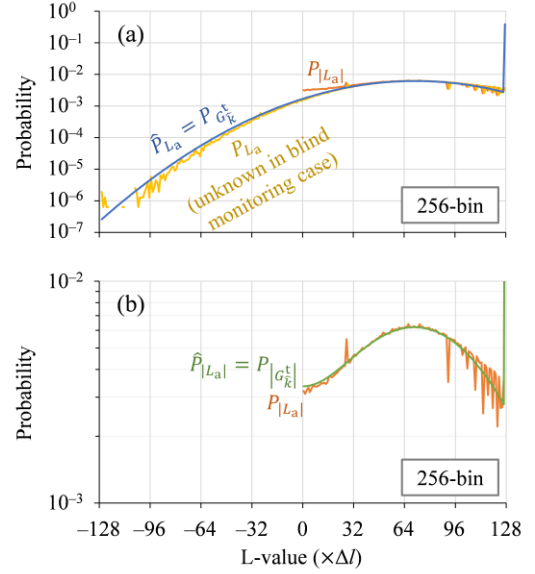


Fig. 3. Exemplified histogram of L-values for PS-64-QAM having $\mathbb{H}(\mathbf{B})$ of 4.1 bpcu and the SNR of 10 dB. The pmfs are as a function of (a) symmetrized *a posteriori* L-value L_a and (b) absolute value $|L_a|$, where $\Delta l = 1/13$. Without the knowledge of the transmitted bits, we know the histogram $P_{|L_a|}(l)$ in (b). In the proposed method, we compare $P_{|L_a|}(l)$ with candidate histograms $P_{|G_k^*|}$ for $k = 1, \dots, K$, and choose the best k , i.e., \hat{k} in (14).

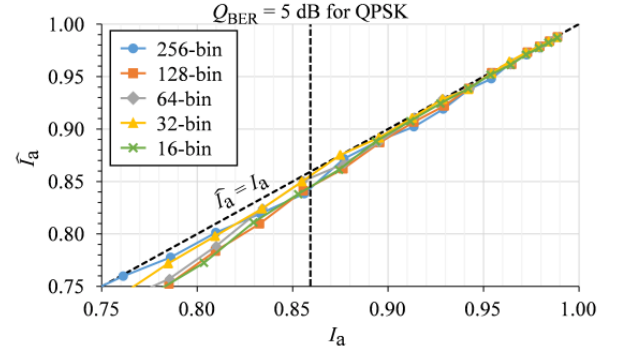


Fig. 4. Performance of ASI estimation for different n_{bin} values for PS-64-QAM having a symbol entropy $\mathbb{H}(\mathbf{B})$ of 4.1 bpcu over the Gaussian channel.

When computing $\mathbb{H}(L_a | |L_a|)$ in (10) in step 6, $P_{|L_a|}$ can be used instead of $\hat{P}_{|L_a|}$ to compute \hat{I}_a . In our simulations, we did not see any significant difference between these two cases.

IV. EXPERIMENTS

We examined the estimation accuracy of the proposed blind performance monitoring method over fiber-optic channels by recirculating loop transmission and back-to-back noise loading experiments.

A. Transmission experiments

The experimental setup is shown in Fig. 5. At the transmitter, we used an electro-optic frequency comb with 51 tones spaced at 25 GHz seeded by an external cavity laser (ECL). The lines were separated by an optical interleaver (OI) into even and odd channels which were each modulated by

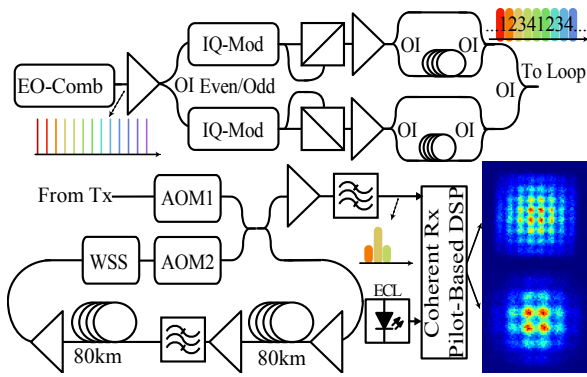


Fig. 5. Experimental setup. Insets are recovered constellations for PS-64-QAM in the case of $\mathbb{H}(\mathbf{B}) = 5.7$ bpcu after 5 roundtrips (top) and $\mathbb{H}(\mathbf{B}) = 4.6$ bpcu after 13 roundtrips (bottom).

an in-phase and quadrature modulator (IQ-Mod) driven by a 60 GS/s arbitrary waveform generator. The symbol rate of the channels was 24 Gbaud. We emulated polarization division multiplexing by a split-delay-combine technique with about 250 symbols delay. Every second of the dual-polarization odd and even channels was further decorrelated with another set of OIs and decorrelation fibers corresponding to about 750 symbols delay to generate a 1–2–3–4–1–2... decorrelation pattern. All channels were then multiplexed and coupled into a recirculating loop using two acousto-optic modulators (AOM). The loop contained two spans of 80 km standard single-mode fiber (SSMF) and the default total input power was 13 dBm, corresponding to a per-channel launch power of -4 dBm. We examined the launch power dependence under limited conditions before sweeping the number of roundtrips, and we observed that -4 dBm is optimal for 5–20 roundtrips (800–3200 km). With the dispersion-uncompensated link in this experiment, the optimal launch power is almost the same even if the number of spans differs. With this default launch power, a moderate amount of fiber nonlinearity influenced the signal quality. Three in-loop erbium-doped fiber amplifiers (EDFAs) with a noise figure of approximately 5 dB compensated for fibre losses and an optical bandpass filter and a wavelength selective switch were employed for rejection of out-of-band ASE noise and compensation of gain tilt. At the receiver the signal was coherently detected by mixing with a local oscillator from another ECL. Receiver side DSP was performed by offline processing; after static chromatic dispersion compensation, we performed fully pilot-aided signal recovery [48].⁶ The adaptive equalization consisted of butterfly-structured finite-impulse-response filters with 45 half-symbol taps based on the constant modulus algorithm of the pilot sequence with a length of 2048 symbols. The carrier phase was estimated by linear interpolation of the phases of interleaved pilot symbols (one per 64 symbols). Examples of recovered constellations are shown in the insets of Fig. 5.

⁶Alternatively, one can estimate the signal quality based on pilot symbols. However, such estimates will not be representative for the whole signal, since pilot symbols usually have a low-order modulation format (in our case, QPSK) without FEC coding, whereas higher-order modulation and FEC are applied to data symbols. Furthermore, the accuracy of pilot-based signal quality estimates is relatively low, since the pilot insertion ratio is usually limited to a few % in deployable systems not to reduce the throughput of the main signal.

We investigated 16-QAM, 64-QAM, PS-16-QAM, PS-64-QAM, and PS-256-QAM. PS-64-QAM signals with $\mathbb{H}(\mathbf{B}) = 4.1, 4.6, 5.2,$ and 5.7 bpcu were generated by CCDD [46]. PS-16-QAM and PS-256-QAM signals were generated with the PS coding method from [49] for $\mathbb{H}(\mathbf{B}) = 3.4, 5.0,$ and 6.3 bpcu, respectively. The SNR of the auxiliary channel was set to a pre-set value per modulation/shaping format at an FEC threshold ASI of FT#1: 0.93, FT#2: 0.86, or FT#3: 0.78 regardless of the number of roundtrips. The number of L-value bins n_{bin} was set to 32 as a reasonable value for practical DSP. To observe one histogram of L-values, we stored 10^5 polarization-multiplexed QAM symbols. The number of examined Gaussian distributions K in the proposed scheme was 8192 (see Sec. III-B, step 1).

Fig. 6 shows the ASI as a function of the launch power based on knowledge of the transmitted bits (solid lines, I_a) and with the proposed method without such knowledge (dotted lines, \hat{I}_a) in selected cases. The modulation/shaping parameters were 16-QAM, PS-64-QAM with $\mathbb{H}(\mathbf{B}) = 5.0$ bpcu, and 64-QAM. The assumed FEC threshold was FT#2. In the examined cases, around -4 dBm/ch is optimal. Except for the case of very low performance of 16-QAM with 20 roundtrips and -1 dBm/ch, the maximum absolute estimation error is 0.036 for 16-QAM with 15 roundtrips and -1 dBm/ch. Above the assumed FEC threshold FT#2, the estimation errors are much smaller.

Fig. 7 shows the ASI as a function of roundtrips for eight modulation/shaping parameters under FT#2 and a launch power of -4 dBm/ch. We can see that the I_a and \hat{I}_a are well correlated, although \hat{I}_a tends to be larger than the true values in the regime shown in Fig. 7.

Fig. 8 shows the relationship between the true and estimated values of (a) ASI or (b) Q-factor under the assumed FEC threshold ASIs. Note that the Q-factor is computed by (17), which is a byproduct of the proposed ASI estimation method. In Fig. 8(a), the estimation in the regime where I_a is larger than or equal to the assumed FEC threshold, the estimation errors are small. The maximum absolute (and relative) estimation errors are 0.016 (1.7%), 0.021 (2.3%), and 0.028 (3.6%) for FT#1, FT#2, and FT#3, respectively. These estimation errors correspond to within 0.5 dB SNR difference for binary modulation over the Gaussian channel. A reason for the positively biased errors above each FEC threshold in experiments could be the larger gap between the L-value and assumed Gaussian distributions. The L-value distribution for the fiber-optic channel could be different from that of the Gaussian channel due to imperfections of the optical transceiver and the DSP. In the DSP, normalization and quantization around soft demapping will influence the blind estimation results. We observe that the estimation error becomes larger for smaller I_a , especially below the assumed FEC limit. We believe this is due to the fact that the true SNR is significantly smaller than the SNR of the auxiliary channel. For example, the SNR of the auxiliary channel was 3 dB larger than the approximated true SNR in the case of PS-256-QAM after 8 roundtrips. In such cases, the mismatched L-values are significantly larger than the true L-values, which would influence the estimation error.

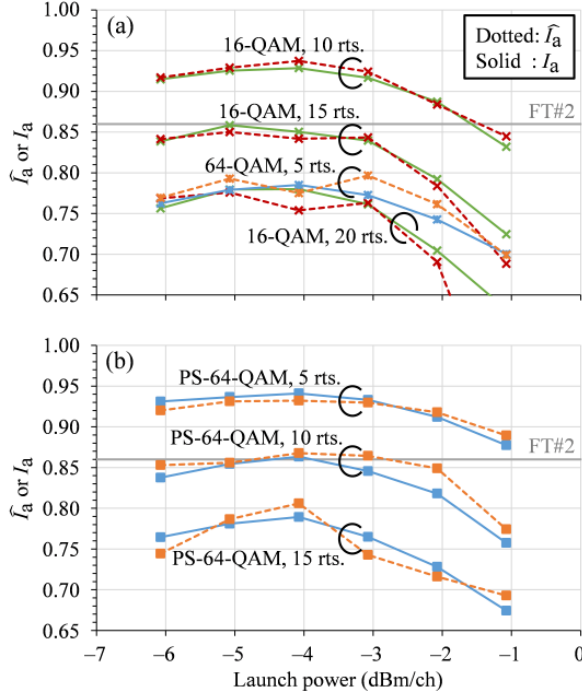


Fig. 6. True and estimated ASI in transmission experiments with varying launch power for (a) uniform 16-QAM (10, 15, and 20 roundtrips) and 64-QAM (5 roundtrips), and (b) PS-64-QAM with $\mathbb{H}(\mathbf{B})$ of 5.0 bpcu (5, 10, and 15 roundtrips).

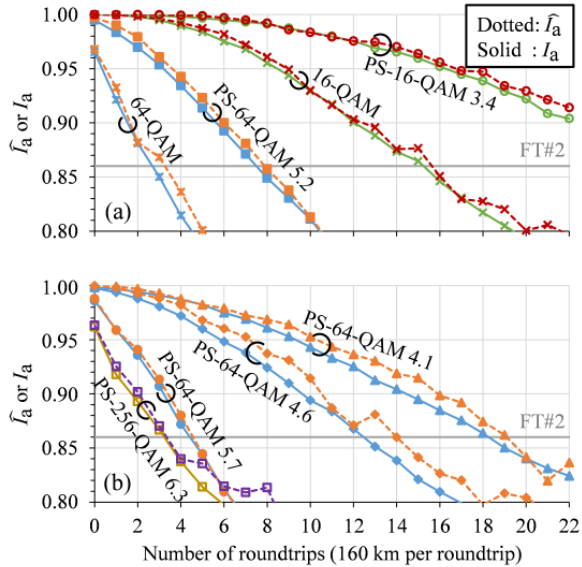


Fig. 7. True and estimated ASI in transmission experiments at a launch power of -4 dBm/ch for (a) PS-16-QAM ($\mathbb{H}(\mathbf{B}) = 3.4$ bpcu), 16-QAM, PS-64-QAM ($\mathbb{H}(\mathbf{B}) = 5.2$ bpcu), and 64-QAM, and (b) PS-64-QAMs ($\mathbb{H}(\mathbf{B}) = 4.1, 4.6, 5.7$ bpcu), and PS-256-QAM ($\mathbb{H}(\mathbf{B}) = 6.3$ bpcu).

We have also tried to estimate the ASI per bit tributary separately and averaged them to obtain a bit-averaged ASI, however this did not improve the estimation accuracy.

Fig. 8(b) depicts the by-product Q-factor estimation error. Similar to the ASI estimate we see a positive bias of the estimated Q-factor $\hat{Q}_{st,L}$. The peak-to-peak estimation error in the Q-factor is within 1.1 dB, 0.8 dB, or 1.5 dB at a Q_{BER} larger than each assumed FEC threshold and lower than 9 dB

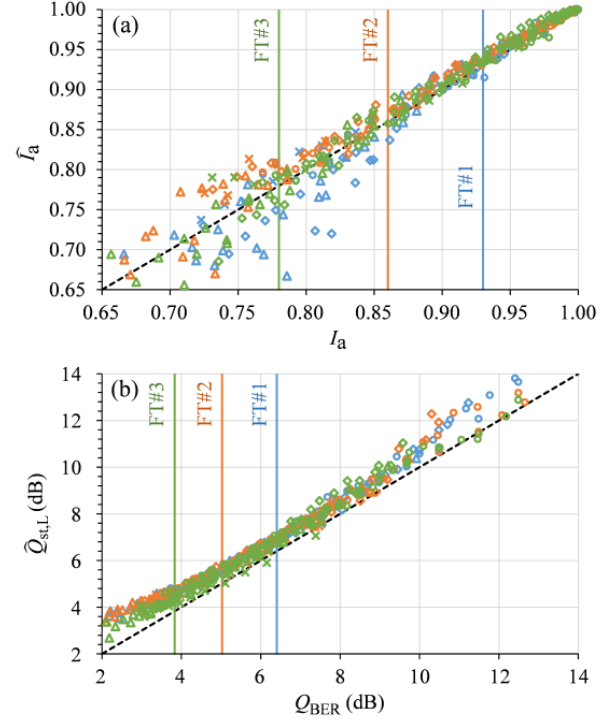


Fig. 8. Estimation errors with the proposed method in (a) soft (ASI) and (b) hard (Q-factor) performance monitoring in transmission experiments. Assumed FEC threshold is FT#1: 0.93 (blue), FT#2: 0.86 (orange), or FT#3: 0.78 (green). The corresponding Q-factors with binary modulation are 6.4 dB, 5.0 dB, or 3.8 dB, respectively. Circles, diamonds, triangles, or crosses depict the cases of 16-QAM and PS-16-QAM, PS-64-QAM with $\mathbb{H}(\mathbf{B}) \leq 5.0$ bpcu, PS-64-QAM with $\mathbb{H}(\mathbf{B}) > 5.0$ bpcu and 64-QAM, or PS-256-QAM, respectively. The dotted line indicates where the estimated value equals to the true value.

(i.e., 3.8–9.0 dB for FT#1, 5.0–9.0 dB for FT#2, or 6.4–9.0 dB for FT#3, respectively). By introducing the correction term $(1 - \rho)$ in (17), the peak-to-peak estimation error in the Q-factor is almost halved. We also observe that $\hat{Q}_{st,L} - Q_{BER}$ depends on the symbol entropy $\mathbb{H}(\mathbf{B})$, i.e., a larger entropy signal such as PS-256-QAM (crosses in the figure) tends to have smaller $\hat{Q}_{st,L} - Q_{BER}$. This dependence was not found in the ASI estimation.

B. Back-to-back experiments

To confirm if the trends observed in the transmission experiments are specific to transmission, we captured and processed data in a back-to-back, noise loading configuration. We swept the OSNR from 10 to 36 dB at 0.1 nm noise bandwidth. Fig. 9 show the estimation errors of (a) ASI and (b) by-product Q-factor. In Fig. 9(a), we see no positive bias of \hat{I}_a over I_a , while the absolute estimation error is comparable with the transmission experiments. In Fig. 9(b), the back-to-back estimated Q-factor exhibits a similar behaviour as in the transmission experiments, i.e., positively bias compared to the true Q_{BER} . The estimation errors are within 1 dB at Q_{BER} of each FEC threshold to 9 dB, which is almost the same as in the transmission experiments. For pure noise-limited situations there would be no specific difference in L-value histograms between the transmission and noise loading cases.

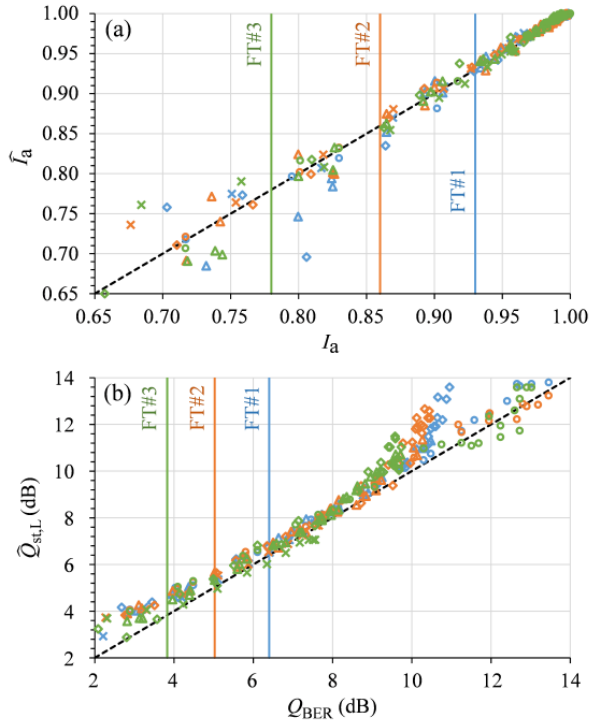


Fig. 9. Estimation errors with the proposed method in (a) soft (ASI) and (b) hard (Q-factor) performance monitoring in B2B noise loading experiments. Legends and colors are the same as in Fig. 8.

However, in the transmission case fiber nonlinearities could cause distribution differences which influences the ASI.

When the ASI is close to 1, the ASI is a highly nonlinear function of SNR (although $\log(-\log(1 - I_a))$ versus SNR is somewhat more linear [42, Fig. 3]). This causes the ASI estimation error to approach zero around $I_a = 1$. It can therefore be said that ASI or other information theoretic metrics are not suitable to quantify the signal performance in this high performance regime, e.g. at SNRs corresponding to $Q_{BER} = 10$ dB. On the other hand, the Q-factor is well suited for this regime, even though the estimation error using our proposed method becomes larger.

V. CONCLUSIONS

We proposed a blind performance monitoring method for systems with soft binary FEC and multilevel modulation. The proposed method estimates the ASI based on a histogram of the *a posteriori* L-values without any knowledge of the transmitted bits. We compare our monitored L-values to a set of Gaussian distribution candidates to approximate them by a Gaussian distribution.

Nine different modulation/shaping formats and three assumed FEC thresholds were examined by middle- to long-haul transmission experiments. We observed positively biased absolute errors, with a maximum estimation error below 0.016 (1.7%), 0.021 (2.3%), or 0.028 (3.6%) for ASIs larger than the assumed FEC threshold of $I_a = 0.78$, 0.86, or 0.93, respectively. This estimation error corresponds to within 0.5 dB SNR difference for binary modulation in the Gaussian channel in the regime of $I_a = 0.78$ –0.93. As a by-product of the

proposed method, we estimated a hard decision performance metric of Q_{BER} . The estimation errors were also positively biased with a maximum absolute error less than 0.8 dB. Finally we investigated the estimation errors with back-to-back noise loading experiments to remove the effects from transmission. Only the ASI exhibits a difference between the two back-to-back and transmission experiments, i.e., the estimated ASI was not positively biased in back-to-back noise loading experiments. Although the mechanism of the estimation bias is not fully clarified, it is likely that the nonlinear fiber transmission changes the L-value distribution away from a Gaussian distribution, inducing an ASI estimation bias. Our proposed method is well suited for performance monitoring in systems carrying live traffic, because only minimal additional functionality is required in the hardware that stores histograms of the L-values before FEC decoding.

ACKNOWLEDGEMENT

We thank Assoc. Prof. Koji Igarashi of Osaka University for fruitful discussions.

REFERENCES

- [1] ITU-T, "Forward error correction for high bit-rate DWDM submarine systems," 2004. [Online]. Available: www.itu.int/rec/T-REC-G.975.1
- [2] ITU-T, "Characteristics of optically amplified optical fibre submarine cable systems," 2015. [Online]. Available: www.itu.int/rec/T-REC-G.977
- [3] S. Oda, M. Miyabe, S. Yoshida, T. Katagiri, Y. Aoki, T. Hoshida, J. C. Rasmussen, M. Birk, and K. Tse, "A learning living network with open ROADMs," *IEEE/OSA J. Lightw. Technol.*, vol. 35, no. 8, pp. 1350–1356, Apr. 2017.
- [4] Z. Dong, F. N. Khan, Q. Sui, K. Zhong, C. Lu, and A. P. T. Lau, "Optical performance monitoring: a review of current and future technologies," *IEEE/OSA J. Lightw. Technol.*, vol. 34, no. 2, pp. 525–543, Jan. 2016.
- [5] D. C. Kilper, R. Bach, D. J. Blumenthal, D. Einstein, T. Landolsi, L. Ostar, M. Preiss, and A. E. Wilner, "Optical performance monitoring," *IEEE/OSA J. Lightw. Technol.*, vol. 22, no. 1, pp. 294–304, Jan. 2004.
- [6] X. Wu, J. A. Jargon, R. A. Skoog, L. Paraschis, and A. E. Wilner, "Applications of artificial neural networks in optical performance monitoring," *IEEE/OSA J. Lightw. Technol.*, vol. 27, no. 16, pp. 3580–3589, Aug. 2009.
- [7] B. Fu, R. Hui, and D. L. Richards, "Optical channel performance monitoring using coherent detection," *Opt. Fib. Commun. Conf. (OFC)*, Anaheim, CA, USA, Mar. 2005, Paper OWJ2.
- [8] F. N. Hauske, M. Kuschnerov, B. Spinnler, and B. Lankl, "Optical performance monitoring in digital coherent receivers," *IEEE/OSA J. Lightw. Technol.*, vol. 27, no. 16, pp. 3623–3631, Aug. 2009.
- [9] R. Adams, M. Rochette, T. T. Ng, and B. J. Eggleton, "All-optical in-band OSNR monitoring at 40 Gb/s using nonlinear optical loop mirror," *IEEE Photon. Technol. Lett.*, vol. 18, no. 3, pp. 469–471, Feb. 2006.
- [10] D. Zhao, L. Xi, X. Tang, W. Zhang, Y. Qiao, and X. Zhang, "Periodic training sequence aided in-band OSNR monitoring in digital coherent receiver," *IEEE Photonics Journal*, vol. 6, no. 4, Aug. 2014.
- [11] G. Bosco, V. Curri, A. Carena, P. Poggiolini, and F. Forghieri, "On the performance of Nyquist-WDM Terabit superchannels based on PM-BPSK, PM-QPSK, PM-8QAM or PM-16QAM subcarriers," *IEEE/OSA J. Lightw. Technol.*, vol. 29, no. 1, pp. 53–61, Jan. 2011.
- [12] O. V. Sinkin, J.-X. Cai, D. G. Foursa, G. Mohs, and A. N. Pilipetskii, "Impact of broadband four-wave mixing on system characterization," *IEEE/OSA Opt. Fib. Commun. Conf. and Exposition and The Natl. Fib. Opt. Eng. Conf. (OFC/NFOEC)*, Anaheim, CA, USA, Mar. 2013, Paper OM2B.4.2013, Paper OTH3G.3.
- [13] Y. Xiang, M. Tang, Q. Wu, H. Zhou, B. Yong, S. Fu, D. Liu, "A joint OSNR and nonlinear distortions estimation method for optical fiber transmission system," *IEEE Photonics Journal*, vol. 10, no. 5, Sep. 2018.
- [14] A. S. Kashi, Q. Zhuge, J. C. Cartledge, S. Ali Etemad, A. Borowiec, D. W. Charlton, C. Laperle, and M. O'Sullivan, "Nonlinear signal-to-noise ratio estimation in coherent optical fiber transmission systems using artificial neural networks," *IEEE/OSA J. Lightw. Technol.*, vol. 36, no. 23, pp. 5424–5431, Dec. 2018.

- [15] T. Tanimura, K. Tajima, S. Yoshida, S. Oda, and T. Hoshida, "Experimental demonstration of a coherent receiver that visualizes longitudinal signal power profile over multiple spans out of its incoming signal," in *Proc. Eur. Conf. Opt. Commun. (ECOC)*, Dublin, Ireland, Sep. 2019, Paper PD.3.4.
- [16] N. S. Bergano, F. W. Kerfoot, and C. R. Davidson, "Margin measurement in optical amplifier systems," *IEEE Photon. Technol. Lett.*, vol. 5, no. 3, pp. 304–306, Mar. 1993.
- [17] L. Song, M.-L. Yu, and M. S. Shaffer, "10- and 40-Gb/s forward error correction devices for optical communications," *IEEE J. Solid-state circuits*, vol. 37, no. 11, pp. 1565–1573, Nov. 2002.
- [18] K. Roberts, M. O'Sullivan, K.-T. Wu, H. Sun, A. Awadalla, D. J. Krause, and C. Laperle, "Performance of dual-polarization QPSK for optical transport systems," *J. Lightw. Technol.*, vol. 27, no. 16, pp. 3546–3559, Aug. 2009.
- [19] F. Chang, K. Onohara, and T. Mizuochi, "Forward error correction for 100 G transport networks," *IEEE Commun. Mag.*, vol. 48, no. 3, pp. S48–S55, Mar. 2010.
- [20] A. Alvarado, T. Fehenberger, B. Chen, F. M. J. Willems, "Achievable information rates for fiber optics: applications and computations," *IEEE/OSA J. Lightw. Technol.*, vol. 36, no. 2, pp. 424–439, Jan. 2018.
- [21] G. Böcherer, F. Steiner, and P. Schulte, "Bandwidth efficient and rate-matched low-density parity-check coded modulation," *IEEE Trans. Commun.*, vol. 63, no. 12, pp. 4651–4665, Dec. 2015.
- [22] F. Buchali, F. Steiner, G. Böcherer, L. Schmalen, P. Schulte, and W. Idler, "Rate adaptation and reach increase by probabilistically shaped 64-QAM: an experimental demonstration," *IEEE/OSA J. Lightw. Technol.*, vol. 34, no. 7, pp. 1599–1609, Apr. 2016.
- [23] L. Schmalen, A. Alvarado, and R. Rios-Müller, "Performance prediction of nonbinary forward error correction in optical transmission experiments," *IEEE/OSA J. Lightw. Technol.*, vol. 35, no. 4, pp. 1015–1027, Feb. 2017.
- [24] A. Alvarado, E. Agrell, D. Lavery, R. Maher, and P. Bayvel, "Replacing the soft FEC limit paradigm in the design of optical communication systems," *IEEE/OSA J. Lightw. Technol.*, vol. 33, no. 20, pp. 4338–4352, Oct. 2015.
- [25] J. Cho, L. Schmalen, and P. J. Winzer, "Normalized generalized mutual information as a forward error correction threshold for probabilistically shaped QAM," in *Proc. Eur. Conf. Opt. Commun. (ECOC)*, Gothenburg, Sweden, Sep. 2017, Paper M.2.D.2.
- [26] G. Böcherer, "Achievable rates for probabilistic shaping," [Online]. Available: arxiv.org/abs/1707.01134
- [27] T. Yoshida, M. Karlsson, and E. Agrell, "Performance metrics for systems with soft-decision FEC and probabilistic shaping," *IEEE Photon. Technol. Lett.*, vol. 29, no. 23, pp. 2111–2114, Dec. 2017.
- [28] G. Böcherer, P. Schulte, and F. Steiner, "Probabilistic shaping and forward error correction for fiber-optic communication systems," *IEEE/OSA J. Lightw. Technol.*, vol. 37, no. 2, pp. 230–244, Jan. 2019.
- [29] T. Yoshida, M. Mazur, J. Schröder, M. Karlsson, E. Agrell, "Performance monitoring for live systems with soft FEC," in *Proc. Eur. Conf. Opt. Commun. (ECOC)*, Dublin, Ireland, Sep. 2019, Paper W.3.D.5.
- [30] S. Zhang, F. Yaman, E. Mateo, I. B. Djordjevic, K. Nakamura, T. Inoue, and Y. Inada, "On the performance metric and design of non-uniformly shaped constellation," in *Proc. Opt. Fib. Commun. Conf. (OFC)*, San Diego, CA, USA, Mar. 2019, Paper W1D.7.
- [31] T. Yoshida, M. Karlsson, and E. Agrell, "Technologies toward implementation of probabilistic constellation shaping," in *Proc. Eur. Conf. on Opt. Comm. (ECOC)*, Rome, Italy, Sep. 2018, Paper Th.1.H.1.
- [32] T. Yoshida, M. Karlsson, and E. Agrell, "Hierarchical distribution matching for probabilistically shaped coded modulation," *IEEE/OSA J. Lightw. Technol.*, vol. 37, no. 6, pp. 1579–1589, Mar. 2019.
- [33] A. Amari, S. Goossens, Y. C. Gültekin, O. Vassilieva, I. Kim, T. Ikeuchi, C. Okonkwo, F. M. J. Willems, and A. Alvarado, "Introducing enumerative sphere shaping for optical communication systems with short blocklengths," [Online]. Available: <https://arxiv.org/pdf/1904.06601v3>
- [34] E. Zehavi, "8-PSK trellis codes for a Rayleigh channel," *IEEE Trans. Commun.*, vol. 40, no. 3, pp. 873–884, May 1992.
- [35] G. Caire, G. Taricco, and E. Biglieri, "Bit-interleaved coded modulation," *IEEE Trans. Inf. Theory*, vol. 44, no. 3, pp. 927–946, May 1998.
- [36] A. Guillén i Fàbregas, A. Martinez, and G. Caire, "Bit-interleaved coded modulation," *Found. Trends Commun. Inf. Theory*, vol. 5, nos. 1/2, pp. 1–153, 2008.
- [37] L. Szczecinski and A. Alvarado, *Bit-Interleaved Coded Modulation: Fundamentals, Analysis, and Design*. Chichester, UK, John Wiley & Sons, 2015.
- [38] OIF, "400ZR," [Online]. Available: www.oiforum.com/technical-work/hot-topics/400zr-2/
- [39] Open ROADM MSA, [Online]. Available: www.openroadm.org/home.html
- [40] I. Lyubomirsky, B. Smith, J. Riani, S. Bhoja, G. Nicholl, M. Nowell, F. Villarruel, "400G FEC and framing for 80 km," [Online]. Available: www.grouper.ieee.org/groups/802/3/B10K/public/18_09/lyubomirsky_b10k_01a_0918.pdf
- [41] J. Cho and P. J. Winzer, "Probabilistic constellation shaping for optical fiber communications," *IEEE/OSA J. Lightw. Technol.*, vol. 37, no. 6, pp. 1590–1607, Mar. 2019.
- [42] T. Yoshida, A. Alvarado, M. Karlsson, and E. Agrell, "Post-FEC BER prediction for bit-interleaved coded modulation with probabilistic shaping," [Online]. Available: arxiv.org/abs/1911.01585
- [43] T. Yoshida, M. Mazur, J. Schröder, M. Karlsson, and E. Agrell, "On the performance under hard and soft bitwise mismatched-decoding," in *Proc. Opt. Fib. Commun. Conf. (OFC)*, San Diego, CA, Mar. 2020, Paper Th11.5.
- [44] G. Kaplan and S. Shamai, "Information rates and error exponents of compound channels with application to antipodal signaling in a fading environment," *Archive for Electronics and Transmission Technique (Archiv für Elektronik und Übertragungstechnik, AEU)*, vol. 47, no. 4, pp. 228–239, 1993.
- [45] T. Yoshida, K. Matsuda, K. Kojima, H. Miura, K. Dohi, M. Pajovic, T. Koike-Akino, D. S. Millar, K. Parsons, and T. Sugihara, "Hardware-efficient precise and flexible soft-demapping for multi-dimensional complementary APSK signals," in *Proc. Eur. Conf. Opt. Commun. (ECOC)*, Düsseldorf, Germany, Sep. 2016, Paper Th.2.P2.SC3.27.
- [46] P. Schulte and G. Böcherer, "Constant composition distribution matching," *IEEE Trans. Inf. Theory*, vol. 62, no. 1, pp. 430–434, Jan. 2016.
- [47] K. Sugihara, Y. Miyata, T. Sugihara, K. Kubo, H. Yoshida, W. Matsumoto, and T. Mizuochi, "A spatially-coupled type LDPC code with an NCG of 12 dB for optical transmission beyond 100 Gb/s," in *Proc. Opt. Fib. Commun. Conf. (OFC)*, Anaheim, CA, USA, Mar. 2013, Paper OM2B.4.
- [48] M. Mazur, J. Schröder, A. Lorences-Riesgo, T. Yoshida, M. Karlsson, and P. A. Andrekson, "Overhead-optimization of pilot-based digital signal processing for flexible high spectral efficiency transmission," *OSA Opt. Express*, vol. 27, no. 17, pp. 24654–24669, Aug. 2019.
- [49] T. Yoshida, M. Karlsson, and E. Agrell, "Low-complexity variable-length output distribution matching with periodical distribution uniformization," in *Proc. Opt. Fib. Commun. Conf. (OFC)*, San Diego, CA, Mar. 2018, Paper M4E.2.